Nanoscale

Accepted Manuscript

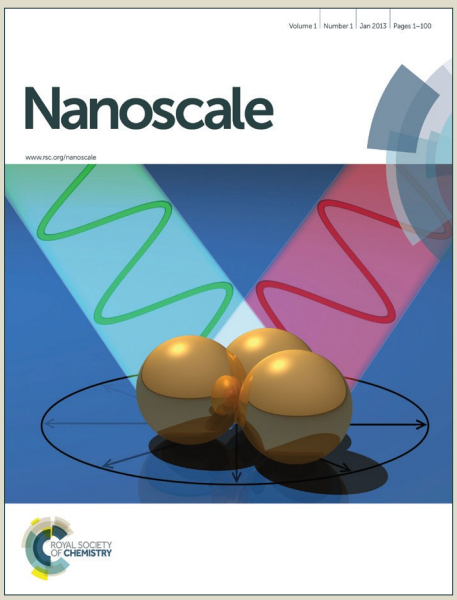

ROYAL SOCIETY OF CHEMISTRY

www.rsc.org/nanoscale

TOC graphic

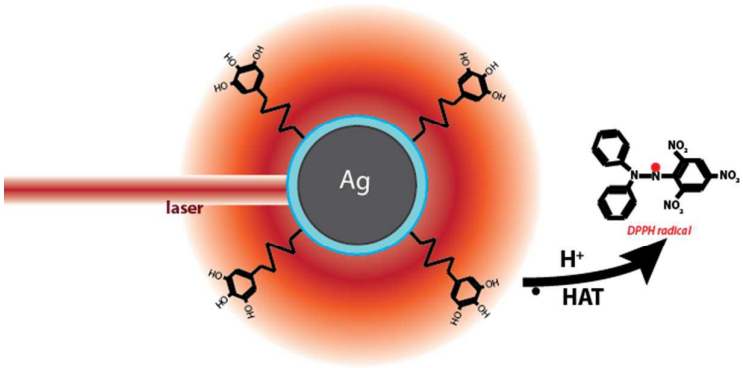

The proton-coupled electron transfer from gallic acid molecules immobilized on silica coated plasmonic Ag nanoparticles is enhanced by near-infrared laser irradiation.

Nanoantioxidant-driven plasmon enhanced proton-coupled electron transfer

Georgios A. Sotiriou[1,2], *Christoph O. Blattmann*[1], *Yiannis Deligiannakis*[1,3]*

[1]Particle Technology Laboratory, Institute of Process Engineering, Department of Mechanical and Process Engineering, ETH Zurich, Sonneggstrasse 3, CH-8092, Zurich, Switzerland.
[2]Drug Formulation & Delivery, Institute of Pharmaceutical Sciences, Department of Chemistry and Applied Biosciences, ETH Zurich, Vladimir-Prelog-Weg 3, CH-8093, Zurich Switzerland.
[3]Laboratory of Physical Chemistry and Materials, Department of Physics, University of Ioannina, 45110 Ioannina, Greece.

*Corresponding author: Y. Deligiannakis, ideligia@cc.uoi.gr

22 September 2015

Submitted to: *Nanoscale*

TOC graphic

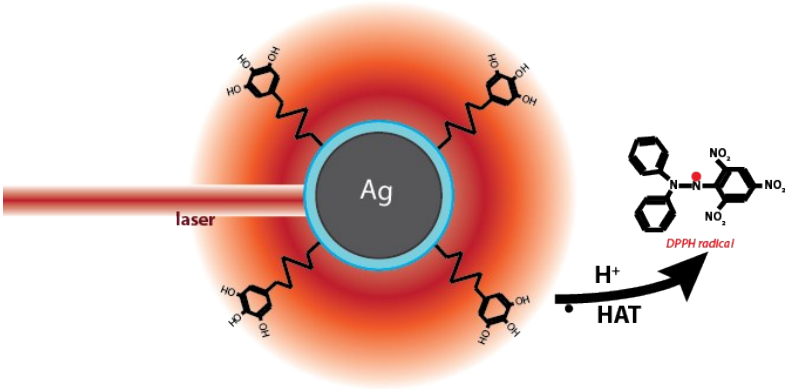

The proton-coupled electron transfer from gallic acid molecules immobilized on silica coated plasmonic Ag nanoparticles is enhanced by near-infrared laser irradiation.

ABSTRACT

Proton-coupled electron transfer (PCET) reactions involve the transfer of a proton and an electron and play an important role in a number of chemical and biological processes. Here, we describe a novel phenomenon, plasmon-enhanced PCET, which is manifested using SiO_2-coated Ag nanoparticles functionalized with gallic acid (GA), a natural antioxidant molecule that can perform PCET. These GA-functionalized nanoparticles show enhanced plasmonic response at near-IR wavelengths, due to particle agglomeration caused by the GA molecules. Near-IR laser irradiation induces strong local hot-spots on the SiO_2-coated Ag nanoparticles, as evidenced by surface enhanced Raman scattering (SERS). This leads to plasmon energy transfer to the grafted GA molecules. That lowers the GA-OH bond dissociation enthalpy by at least 2 kcal/mole and therefore facilitates PCET. The nanoparticle-driven plasmon-enhancement of PCET brings together the so far unrelated research domains of nanoplasmonics and electron/proton translocation with significant impact on applications based on interfacial electron/proton transfer.

Keywords: plasmonic, PCET, core-shell, gallic, nanoantioxidant, near-infrared, nanosilver.

INTRODUCTION

Hydrogen atom $H^{\bullet}$ ($\equiv H^{+} + e^{-}$) transfer (HAT) is a reaction that involves the transfer of a proton and an electron.[1-2] HAT reactions are involved in a number of chemical and biological processes,[3] and belong to the most important proton-coupled electron transfer (PCET) reactions.[4-7] Organic HAT reactions have been studied for over a century[4,8] and thousands of kinetic rate constants have been determined.[9-10] At similar conditions, HAT reactions from O–H bonds are significantly faster than those involving C–H bonds.[11] Therefore phenolic molecules have been established among the most efficient antioxidants operating *via* the HAT mechanism.[8-9]

So far, PCET/HAT have been observed exclusively in chemical systems comprised of organic molecules containing metal complexes[1] in appropriate solvents or biological systems.[4,12] Scrauben et al.[13] demonstrated that metal-oxide nanoparticles, such as TiO_2 and ZnO, can perform HAT. This discovery was the first example where metal oxide surfaces can act as a PCET reagent and has implications for the understanding and development of chemical energy technologies that depend on e^{-}/H^{+} transfer.[13] Recently, we have shown that highly efficient *hybrid* nanoantioxidant materials can be created by functionalization of SiO_2 nanoparticles with natural antioxidant molecules of gallic acid (GA).[14] These SiO_2-GA nanoparticles perform rapid HAT from the OH groups of GA to 2,2-diphenyl-1-picrylhydrazyl radicals ($DPPH^{\bullet}$).[14] SiO_2 nanoparticles provide a modular support for covalent grafting of the antioxidant while the nanosize enables the control of the secondary HAT reactions.[14]

Plasmonic materials such as Ag have attracted a great deal of attention due to their strong potential in a variety of fields including energy,[15] catalysis,[16] optoelectronics,[17] and biomedical applications.[18] The rationale behind the interest to design novel plasmonic nanoplatforms is based on the ability of plasmonic nanoparticles to absorb and scatter light at specific wavelengths.[19] This property results in two types of fundamental phenomena. First, the interaction of metal nanoparticles with light generates an intense electric field on their surface, which is useful for a number of plasmon-enhanced reactions including water splitting[20], oxidation[21], and hydrocarbon conversion.[22] Second, when plasmonic nanoparticles are excited on resonance, energy is either radiated through light scattering or is dissipated through non-radiative Landau damping generating heat.[23-24] This heat generation process finds applications in photothermal oncology treatment,[25] controlled drug release[26] and bioimaging.[27] Recently, Neumann et al.[24] demonstrated that aqueous suspension of gold nanoparticles facilitates vapor generation from solar irradiation by exploiting

this plasmonic photothermal phenomenon. Both the radiative and non-radiative processes can be controlled by parameters such as the plasmonic-particle size, surface shape and agglomeration state.[28]

Silver nanoparticles, have the lowest plasmonic losses in the UV-visible spectrum.[29] However, a major drawback is their surface oxidation and - in the presence of halogens - halide formation.[19] Surface oxidation leads to its subsequent Ag_2O dissolution in aqueous solutions[30] by releasing toxic[31] Ag^+ ions, while halide formation can reduce significantly the plasmonic performance.[19] Recently we have demonstrated that the Ag^+ ion release of Ag nanoparticles can be minimized, essentially eliminating their toxicity, by hermetically encapsulating them with a nanothin amorphous SiO_2 layer.[32] The SiO_2 shell on Ag nanoparticles offers distinct advantages: (i) it prevents Ag^+ ion release or leaching, (ii) prevents potential charge transfer phenomena from the metallic nanoparticle to an organic molecule on its surface, (iii) facilitates dispersion of metallic nanoparticles without organic surface functionalization and (iv) SiO_2-coated Ag nanoparticles retain their plasmonic properties.[32]

Here, a novel approach is presented that exploits plasmonic resonance to enhance HAT (or PCET) by GA-functionalized, SiO_2-coated Ag nanoparticles, as depicted in Figure 1. These hybrid nanoparticles can efficiently perform HAT towards stable $DPPH^{\bullet}$ that acts as H-atom acceptor.[14] Most importantly, it is shown that the plasmonic HAT enhancement takes place under biologically relevant near-IR laser excitation (785 nm), where human tissue has the highest transmittance.[33] This nanoparticle-driven plasmon-enhancement of PCET brings together the so far unrelated domains of nanoplasmonics and electron/proton translocation, and promises significant impact on a variety of applications including antioxidant technology.[34]

MATERIALS AND METHODS

Nanoparticle production and characterization

SiO_2-coated silver nanoparticles were made in the gas phase using a modified enclosed flame spray reactor, as described in detail elsewhere.[32,35] In brief, a liquid precursor solution consisting of Ag-acetate (0.5 M, Sigma Aldrich, purity 99%) in 2-ethylhexanoic acid (Sigma Aldrich, purity ≥99%) and acetonitrile (Sigma Aldrich, purity ≥99%) at a volume ratio 1:1 was fed through the flame spray pyrolysis nozzle (5 mL/min) and atomized by 5 L/min O_2 (PanGas, purity >99.9%, flow rate: 5 L/min) forming a fine spray. This spray was ignited by a premixed CH_4/O_2 (1.5/3.2 L/min) flame. The reactor was enclosed by a 20 cm quartz glass tube. On top of that tube, a metallic ring with 16 equidistant openings was placed. Through

these openings, Si precursor vapor (hexamethyldisiloxane-HMDSO, Sigma Aldrich, purity ≥99%) was injected along with 15 L/min N_2. The reactor was terminated by another 30 cm quartz glass tube. The Si precursor vapor was supplied by flowing N_2 through a liquid HMDSO-containing bubbler.

Covalent grafting of GA on SiO_2-coated Ag nanoparticles

The functionalization protocol used in this work has been fully detailed in our recent work.[14] This results in covalent grafting of the GA molecule on the SiO_2-coated Ag particle *via* a peptide bond (Scheme S1 in Supporting Information) as proven by the FTIR data (Supporting Information, Figure S1) in KBr pellets using a PerkinElmer 580 spectrophotometer. The GA functionalization step involves a washing phase (3 times with acetone, 3 times methanol) that removes any non-covalently attached GA. Thermogravimetric analysis was performed with a Netzsch STA 449 C Jupiter coupled to a Netzsch QMS 403C mass spectrometer (MS).

Nanoparticles were imaged with a high-resolution transmission electron microscope (Tecnai F30, FEI; LaB6 cathode, operated at 300 kV, point resolution ~2 Å). X-ray diffraction (XRD) patterns were obtained with a Bruker AXS D8 Advance spectrometer (Cu Kα, 40 kV, 40 mA). The crystal size of silver was determined using the TOPAS 3 software and fitting only the (111) main diffraction peak (2θ = 36°–40°) with the Inorganic Crystal Database [ICSD Coll. Code.: 064995]. UV-visible optical absorption measurments were performed with a Varian Cary 500. The nanoparticles were dispersed in methanol and measured in a quartz cuvette (optical path 1 cm) with pure methanol as a background. Photothermal heating experiments were performed on the aforementioned suspensions using a near-IR 785 nm diode laser with tunable power (IRM785TA-3000FC, SLOC Lasers, 5mm beam diameter). Size distributions of particles in methanol solutions were obtained by dynamic light scattering (DLS, Zetasizer, Malvern Instruments). The photothermal heating was measured by irradiating PMMA cuvettes of the methanol solutions containing the particles with the near-IR laser while their temperature was monitored over time with an infrared camera (Fluke, Ti110).

Antioxidant evaluation

$DPPH^{\bullet}$ decay kinetics measurements were performed using a Varian Cary 500 spectrophotometer in methanol solutions. The intensity at 515 nm was monitored over time. The effect of the laser irradiation on

the DPPH$^{\bullet}$ decay kinetics was evaluated by irradiating the cuvette with 10 s pulses. Bulk heating temperatures were performed using an Agilent Cary 50 with a temperature controlled cuvette holder. Raman specta were collected using a Renishaw spectrophotometer and a 785 nm laser (max power 500 mW) and a 5x objective, NA = 0.12). Electron Paramagnetic Resonance (EPR) spectra were recorded with a Bruker ER200D spectrometer at 77K (in liquid-N_2), equipped with an Agilent 5310A frequency counter. Adequate signal-to-noise was obtained after 10 scans.

RESULTS AND DISCUSSION

Hybrid nanoparticle morphology

Ag nanoparticles (40 nm in diameter) hermetically encapsulated by a nanothin (1-2 nm) amorphous SiO_2 (5 wt%) shell, Figure 1a, were made by enclosed flame spray pyrolysis.[32] This synthetic route allows for precise control of the SiO_2 shell thickness,[35] a prerequisite for the antioxidant performance of nanoparticles as it is demonstrated hereafter. The SiO_2 surface was further functionalized with GA[14] (Scheme in Figure 1), which is the antioxidant molecule with the highest activity among all polyphenols.[36] The core-shell nanostructure is not altered by the covalent grafting of GA on the SiO_2 surface, as evidenced by TEM images (Figure 1b). The SiO_2 shell remains intact after surface functionalization that involved an initial formation of amine groups (-NH_2) on the SiO_2 surface and a subsequent GA grafting by reaction.[14] This results in covalently grafted GA molecules to the SiO_2 surface *via* a peptide bond as verified by FTIR (Supporting Information, Figure S1 at 1628 and 1705 cm^{-1}). Thermogravimetric analysis (TGA) shows that the organic loading in GA-functionalized SiO_2-coated Ag nanoparticles is 0.3 wt%. Furthermore, these surface functionalization reactions do not cause any Ag-core degradation or etching, evidenced by the identical X-ray diffraction patterns and the deduced 40 nm Ag crystal sizes of the as-prepared (black line) and functionalized (red line) particles shown in Figure 1c.

Electron Paramagnetic Resonance (EPR) data (Supporting Information, Figure S2) show that the grafted GA molecules, when exposed to alkaline pH 12, stabilize monomeric radicals. The g-value 2.0040 is characteristic for radicals localized on the phenolic oxygen of GA immobilized on SiO_2 nanoparticles.[14] This demonstrates that the phenolic OH groups retain their ability to relay protons and electrons, which is a crucial prerequisite for the antioxidant activity of grafted GA molecules.[14] Furthermore, the above EPR spectrum reveals a narrow signal characteristic for metallic Ag^0 at g = 1.992.[37]

Plasmonic photothermal effect

The optical absorption spectrum of as-prepared Ag-SiO_2 core-shell nanoparticles (black line) shows a dominant mode centered around the plasmon resonance frequency of Ag at 409 nm[32] (Figure 2a). In a methanolic suspension this results in a bright-yellow color (Figure 2a, left inset). On the other hand, the GA-functionalized, SiO_2-coated Ag nanoparticles show a characteristic difference in their absorption spectrum (red line). The main peak at 409 nm is attenuated with a concomitant spreading of the absorbance at higher wavelengths with a maximum shoulder at 580 nm. This results in a color-change to purple-pink of those nanoparticles in methanol (Figure 2a, right inset). This plasmonic spectral modification is analogous to that observed for SiO_2-coated Ag nanoparticles agglomerated by adsorbed aminopyrene molecules[38] and of aggregated Au nanoparticles.[39] Here, the GA functionalization induces agglomeration of SiO_2-coated Ag nanoparticles according to the increased average hydrodynamic diameter in methanol from 150 to 310 nm as determined by dynamic light scattering (Supporting Information, Figure S3). Agglomeration promotes plasmonic particle coupling[39] and broadens the plasmonic absorption to the near-IR spectral region[40] (700-1100 nm).

Figure 2b shows the temperature of methanol suspensions in quartz cuvette containing different concentrations of functionalized nanoparticles as a function of laser irradiation time at near-IR (785 nm) with radiative flux (power per area) of 11.7 W/cm^2. Under continuous irradiation, the temperature of the suspension increases and tends to stabilize after 150 s, in agreement with similar observations for plasmonic gold nanoparticles.[39,41] There is a clear particle concentration-dependent photothermal temperature increase from 0.01 to 0.2 mg/mL of Ag. *In situ* recording of the suspension temperature by a thermal camera (Figure 2b, inset) illustrates the spatial heat distribution in the suspension under laser irradiation to depend on particle concentration. This strong temperature increase (ΔT_{max} > 30 ˚C) indicates that the hybrid plasmonic core-shell nanoparticles convert near-IR light to heat through their electron relaxation processes,[42] at a wavelength 500-800 nm far from the typical plasmon resonance frequency of Ag in the near-UV to visible region *i.e.* around 400 nm.[19] It should be noted that the as-prepared core-shell nanoparticles (without surface functionalization) did not exhibit any significant temperature increase upon irradiation because of their minimal absorbance in the near-IR region (Figure 2a) as the silica coating minimizes particle agglomeration.[32] So the gallic acid functionalization step is essential for tuning the absorption spectrum.

HAT by GA functionalized SiO_2-coated Ag nanoparticles

GA drives HAT reactions to stable DPPH$^{\bullet}$ in aprotic (methanol) solutions, when in homogeneous phase[43] as well as when immobilized[14] on SiO_2 nanoparticles. The initial fast-decay of the DPPH radical (DPPH$^{\bullet}$) interacting with a phenolic antioxidant (GA) is due to two rapid reactions [1] and [2]:

$$GA(OH) + DPPH^{\bullet} \rightarrow GA(O^{\bullet}) + H\text{-}DPPH \qquad \text{eq. [1]}$$

$$GA(O^{\bullet}) + DPPH^{\bullet} \rightarrow GA\text{-}Quinone \qquad \text{eq. [2]}$$

These are H-Atom Transfer reactions [HAT] from the phenolic OH groups of GA to the DPPH-radical [14]. As described in detail [14], reaction [1] corresponds to the HAT from one OH of the GA molecule to one DPPH-radical, forming a transient GA semiquinone radical, GA(O$^{\bullet}$). This is a short-lived species since, according to reaction [2] it can react rapidly with a second DPPH-radical to produce a GA-quinone which is a non-radical product. The time-decay of the DPPH$^{\bullet}$ interacting with GA functionalized SiO_2-coated Ag nanoparticles has been monitored by EPR (Figure 3a) and UV-vis spectroscopy (Figure 3b). The DPPH$^{\bullet}$ radical has a fingerprint EPR signal as shown in Figure 3a, whose time-decay clearly shows the conversion of DPPH$^{\bullet}$ to the non-radical DPPH-H due to HAT from GA.[14] We underline that the transient GA(O$^{\bullet}$) radical is not detected in the EPR spectra in Figure 3a, and this indicates that its lifetime is much sorted than the time-window detection limit of the EPR technique, *i.e.* 10 msec in our instrument. The strong absorbance at 514 nm is characteristic of DPPH$^{\bullet}$ in methanol (Figure 3b).[14] In the same context, the time-decay of this signature absorbance of DPPH$^{\bullet}$ in Figure 3b is due to DPPH$^{\bullet}$ scavenging by GA functionalized SiO_2-coated Ag nanoparticles. This DPPH$^{\bullet}$ scavenging is due to HAT from GA to DPPH$^{\bullet}$.[14] Pristine SiO_2-coated Ag nanoparticles (*i.e.* without GA on their surface) have no effect on the DPPH$^{\bullet}$ (not shown). Moreover, we have verified that our 785 nm laser irradiation causes no spectral changes in the DPPH solution in methanol (Figure S4 in Supporting Information). In addition, control experiments *i.e.* for SiO_2@GA particles interacting with DPPH we observe no effect of 785 nm laser in the decay of the DPPH radicals via the HAT kinetics (Figure S5 in Supporting Information).

Figure 3c shows the kinetics of the DPPH$^{\bullet}$ scavenging (black line), monitored *via* the decay of the 514 nm peak. The decay is heterogeneous e.g. comprising an initial rapid phase, attributed to two-electron HAT reactions, followed by a secondary, significantly slower, kinetic phase.[14] For the GA functionalized SiO_2-

coated Ag nanoparticles the initial fast kinetic phase is determined by the two-electron HAT reactions[14]. The slower phase involves radical-radical coupling effects that are irrelevant to the PCET mechanism.[14]

The initial rapid phase of $DPPH^{\bullet}$ scavenging in Figure 3c is due to 2-electron/2-proton reactions per GA molecule.[14] The active electrons and protons come from two of the phenolic OH groups of GA.[14] Accordingly, for a system where the initial concentration of $[DPPH^{\bullet}]_0 \geq [GA]_0$, as in the present experiments, the fast reaction phase -recorded at the first seconds of the reaction- can be described by eq. [3][43]:

$$\frac{[DPPH^{\bullet}]_t}{[DPPH^{\bullet}]_t - ([DPPH^{\bullet}]_0 - [nGA]_0)} = \frac{[DPPH^{\bullet}]_0}{n[GA]_0} e^{k_1([DPPH^{\bullet}]_0 - [GA]_0)t} \qquad \text{eq. [3]}$$

where $[DPPH^{\bullet}]_0$ and $[GA]_0$ represent the initial concentration of $DPPH^{\bullet}$ and GA respectively. The time-dependent concentration of the $DPPH^{\bullet}$ at any time *t* is represented by $[DPPH^{\bullet}]_t$. In eq. [3] 'n' is the stoichiometric factor for the number of hydrogen atoms (e^-/H^+) transferred per GA. For GA in homogeneous HAT reactions[43] as well as for GA immobilized on SiO_2 nanoparticles[14] this stoichiometric factor is n = 2. Thus, the reaction kinetic rates k_1 can be estimated by fitting the initial, fast reaction phase of $DPPH^{\bullet}$ scavenging kinetics using eq. [3]. The full set of fitted kinetics is presented in the Supporting Information, Figure S6. The derived k_1 rates are plotted in Figure 3d *vs.* laser irradiation power.

From Figure 3d it is seen that upon near-IR laser irradiation the $DPPH^{\bullet}$ scavenging kinetics are significantly accelerated. Equally important, the increase in the reaction kinetic rate k_1 is almost linearly correlated with the laser radiative flux, as shown in Figure 3d. Thus, 785 nm laser irradiation causes a significant enhancement of the HAT from the grafted GA molecules to $DPPH^{\bullet}$. There are two potential mechanisms for this effect: (i) a bulk thermal effect *i.e.* since 785 nm laser irradiation can cause bulk heating of the nanoparticle suspension (Figure 2), or (ii) to a plasmonic enhancement of the local electric field *i.e.* plasmonic energy transfer by local hot-spots of SiO_2-coated Ag particles.[38]

Mechanism of plasmon-enhanced HAT: bulk-heating or energy-transfer?

To distinguish the two effects, the $DPPH^{\bullet}$ decay kinetics were evaluated during bulk heating (without laser irradiation) of the suspensions at 35 ˚C (Figure 3c, green line) and 40 ˚C (Figure 3c, blue line). These temperatures are similar to the one achieved photothermally by the laser of a 0.1 mg/ml suspension (Figure 2, reaching up to 42 ˚C), which corresponds to the utilized concentration in these HAT reactions. Bulk

heating resulted in a slight acceleration in the initial DPPH$^{\bullet}$ scavenging, however the kinetics leveled-off (see blue and green lines in Figure 3c). This effect is characteristic of GA-GA radical coupling that results in significant particle-particle agglomeration, as also observed by the drastic increase of their average hydrodynamic diameter to >1 μm (Supporting Information, Figure S3).[14] In contrast, near IR-785 nm laser irradiation has no prominent effect on particle agglomeration (Supporting Information, Figure S3). Thus, bulk heating cannot account for the significant enhancement of the initial k_1 rates observed in Figure 3d. Therefore, it is likely that this effect is observed due to an energy transfer from the plasmonic hot-spots to GA molecules[38] and strong local electric fields upon laser irradiation.

The presence of local plasmonic hot-spots in the GA functionalized SiO_2-coated Ag nanoparticles is verified *via* their surface-enhanced Raman scattering (SERS) spectra. Figure 4 shows the typical Raman spectra of gallic acid powder (purple line) under excitation by a 785 nm laser.[44] The most prominent peaks at 1695 cm^{-1} and 1374 cm^{-1} are well known characteristics of the carboxylic group of GA.[44] When GA is covalently attached on the SiO_2 shell (Figure 4, red line), these features are absent, since the carboxylate is engaged in the formation of the covalent bond on the amine functionalized SiO_2 surface. Most importantly, by varying the 785 nm laser power, a strong enhancement of the Raman spectrum is observed.[45] For example, Figure 4 shows that the GA bands in GA-functionalized SiO_2-coated Ag nanoparticles are resolved using low laser power *i.e.* 3 orders of magnitude lower than that used for GA powder. Figure 4 (red line) also shows that at low laser power, 0.05 mW, the 1624 cm^{-1} band of the phenolic ring of GA is downshifted and split at ~1573 cm^{-1} while the weaker features below 700 cm^{-1} are not resolved. This is attributed to a strong surface-enhanced Raman (SER) effect of the plasmonic Ag core on the grafted GA molecules.[44-45]

Typically such SER by plasmonic particles is due to generation of hot-spots by plasmonic coupling between neighbouring Ag nanoparticles.[44-45] Recently, Shanthil et al.[38] provided experimental evidence that strong local electric field gradients -or hot spots- are efficiently generated in aggregated SiO_2-coated Ag nanoparticles. The local fields developed in the near vicinity of grafted GA molecules located in the 'hot-spot' areas, can be so strong that at high laser power can destroy the organic molecules. Indeed, at laser power >5 mW, the characteristic "carbon cathedral"[45] at ~1580 cm^{-1} appears (Supporting Information, Figure S7), that is a manifestation of strong thermal carbonisation of GA on the SiO_2-coated Ag nanoparticles.

Overall, the present data reveal that GA plays multiple roles in these nanohybrids: (i) GA functionalization induces a pronounced agglomeration of SiO_2-coated Ag nanoparticles. The increased

agglomeration results in a significant broadening of the plasmonic absorption that spreads to the near-IR spectral region (700-1100 nm), (ii) the agglomerated GA-functionalized SiO_2-coated Ag nanoparticles show a significant plasmonic SERS response, creating hot-spots upon excitation with a near-IR 758 nm laser, (iii) upon such excitation, the hot-spots induce remarkable acceleration of HAT from GA to DPPH$^{\bullet}$. Energetic considerations (Supporting Information) reveal that the local electrical oscillations are the main reason for the decrease of the GA-OH bond dissociation enthalpy (BDE) by at least 2 kcal/mole and the activation barrier by ΔE_a = -1.8 kcal/mole (please see Supporting Information for detailed calculations).

In this context, we propose the following mechanism, schematically depicted in Scheme1: the observed plasmon-enhancement PCET from GA to DPPH$^{\bullet}$ is due to evanescent, electric fields localized in the vicinity of the grafted GA molecules. Since the Ag nanoparticles that serve as the source of evanescent light are smaller than the 785 nm wavelength, the GA molecules - as well as nearby solvent methanol molecules - sense the local electric field vibrations (Scheme 1b). This causes distortion within the molecules leading to the generation of lattice vibrations (phonons) that may have two effects: (i) generate oscillating electric dipoles[19] on GA and/or nearby methanol molecules, and (ii) energy dissipation as heat *via* non-radiative processes.[28,46] Since the DPPH$^{\bullet}$ quenching data show that bulk heating is *not* the dominant mechanism that determines the observed acceleration of PCET under 785 nm irradiation, the electric oscillation enhancement is a *local* phenomenon that operates within few nanometers from the particle surface.[19,38] Taking into account the Raman enhancement on GA, we consider that the local electrical oscillations are the main reason for the decrease of BDE by 2 kcal/mole and the activation barrier by ΔE_a = -1.8 kcal/mole that affect both GA as well as the vicinal methanol solvent molecules decreasing the activation energy barrier for the PCET.

CONCLUSIONS

SiO_2-coated Ag nanoparticles offer a versatile platform where antioxidant gallic acid molecules can be grafted covalently, forming a chemically robust nanohybrid. When such nanoparticles are dispersed in suspension, gallic acid functionalization induces a pronounced agglomeration of SiO_2-coated Ag nanoparticles that results in significant broadening of the plasmonic response to the near-IR spectral region (700-1100 nm). These agglomerated GA functionalized SiO_2-coated Ag nanoparticles show a significant plasmonic Surface Enhanced Raman Scattering, which creates hot-spots upon excitation with a near-IR 758 nm laser. Under 758 nm laser irradiation, the hot-spots induce a remarkable acceleration of Hydrogen Atom

Transfer (HAT) from gallic acid to DPPH radicals, due to a lowering of the bond dissociation enthalpy (BDE) of the phenolic OH moieties by at least 2 kcal/mole.

Our present discovery expands the current view of HAT or PCET processes since it has various, so far unforeseen, implications such as plasmonic enhancement of HAT by near-IR laser excitation of nanoparticles. Mayer and coworkers[11] pointed out that a variety of HAT reactions follow the Marcus theory that although originally developed for *electron transfer* processes is also valid for HAT phenomena. Thus, the present discovery is envisaged to open up a new view on the interconnection of Marcus theory with surface plasmon resonance.

ACKNOWLEDGEMENTS

We thank Dr. Frank Krumeich for the electron microscopy measurements at the Scientific Center for Optical and Electron Microscopy (ScopeM) ETH Zurich. This research was supported by the Swiss National Science Foundation (grant no. 200020–126694) and the European Research Council under the European Union's Seventh Framework Program (FP7/2007-2013, ERC grant agreement no. 247283). G.A.S. was supported by a Swiss National Science Foundation *Advanced Researcher* fellowship (grant no. 145392).

REFERENCES

1. J. M. Mayer, *Annu. Rev. Phys. Chem.,* 2004, **55**363-390.
2. J. M. Mayer, *Acc. Chem. Res.,* 2010, **44**(1), 36-46.
3. G. A. Olah, A. Molnar, *Hydrocarbon Chemistry*. Wiley: New York, 1995.
4. R. I. Cukier, D. G. Nocera, *Annu. Rev. Phys. Chem.,* 1998, **49**337-369.
5. N. Iordanova, H. Decornez, S. Hammes-Schiffer, *J. Am. Chem. Soc.,* 2001, **123**(16), 3723-3733.
6. C. Tommos, G. T. Babcock, *Biochim. Biophys. Acta-Bioenerg.,* 2000, **1458**(1), 199-219.
7. S. C. Weatherly, I. V. Yang, H. H. Thorp, *J. Am. Chem. Soc.,* 2001, **123**(6), 1236-1237.
8. S. I. Baskin, H. Salem, *Oxidants, Antioxidants, and Free Radicals*. Taylor & Francis: Washington, DC, 1997.
9. H. Fischer, *Radical Reaction Rates in Liquids*. Landolt-Bornstein New Series (Springer-Verlag) New York, 1984; Vol. 13, subvol. A to E, and 18, subvol. A to E.
10. J. K. Kochi, *Free Radicals*. Wiley: New York, 1973.
11. J. P. Roth, J. C. Yoder, T. J. Won, J. M. Mayer, *Science,* 2001, **294**(5551), 2524-2526.
12. J. Stubbe, W. A. van der Donk, *Chem. Rev.,* 1998, **98**(2), 705-762.
13. J. N. Schrauben, R. Hayoun, C. N. Valdez, M. Braten, L. Fridley, J. M. Mayer, *Science,* 2012, **336**(6086), 1298-1301.

14. Y. Deligiannakis, G. A. Sotiriou, S. E. Pratsinis, *ACS Appl. Mater. Interfaces,* 2012, **4**(12), 6609-6617.
15. P. Nagpal, N. C. Lindquist, S. H. Oh, D. J. Norris, *Science,* 2009, **325**(5940), 594-597.
16. N. Liu, M. L. Tang, M. Hentschel, H. Giessen, A. P. Alivisatos, *Nat. Mater.,* 2011, **10**(8), 631-636.
17. S. Kawata, A. Ono, P. Verma, *Nat. Photon.,* 2008, **2**(7), 438-442.
18. J. N. Anker, W. P. Hall, O. Lyandres, N. C. Shah, J. Zhao, R. P. Van Duyne, *Nat. Mater.,* 2008, **7**(6), 442-453.
19. K. A. Willets, R. P. Van Duyne, *Annu. Rev. Phys. Chem.,* 2007, **58**267-297.
20. D. B. Ingram, S. Linic, *J. Am. Chem. Soc.,* 2011, **133**(14), 5202-5205.
21. W. H. Hung, M. Aykol, D. Valley, W. Hou, S. B. Cronin, *Nano Lett.,* 2010, **10**(4), 1314-1318.
22. W. Hou, W. H. Hung, P. Pavaskar, A. Goeppert, M. Aykol, S. B. Cronin, *ACS Catalysis,* 2011, **1**(8), 929-936.
23. Y. Gao, Z. Yuan, S. Gao, *J. Chem. Phys.,* 2011, **134**(13), 134702.
24. O. Neumann, A. S. Urban, J. Day, S. Lal, P. Nordlander, N. J. Halas, *ACS Nano,* 2013, **7**(1), 42-49.
25. S. Lal, S. E. Clare, N. J. Halas, *Acc. Chem. Res.,* 2008, **41**(12), 1842-1851.
26. A. G. Skirtach, C. Dejugnat, D. Braun, A. S. Susha, A. L. Rogach, W. J. Parak, H. Mohwald, G. B. Sukhorukov, *Nano Lett.,* 2005, **5**(7), 1371-1377.
27. D. Boyer, P. Tamarat, A. Maali, B. Lounis, M. Orrit, *Science,* 2002, **297**(5584), 1160-1163.
28. K. L. Kelly, E. Coronado, L. L. Zhao, G. C. Schatz, *J. Phys. Chem. B,* 2003, **107**(3), 668-677.
29. W. L. Barnes, A. Dereux, T. W. Ebbesen, *Nature,* 2003, **424**(6950), 824-830.
30. G. A. Sotiriou, A. Meyer, J. T. N. Knijnenburg, S. Panke, S. E. Pratsinis, *Langmuir,* 2012, **28**(45), 15929-15936.
31. G. A. Sotiriou, S. E. Pratsinis, *Environ. Sci. Technol.,* 2010, **44**(14), 5649-5654.
32. G. A. Sotiriou, T. Sannomiya, A. Teleki, F. Krumeich, J. Vörös, S. E. Pratsinis, *Adv. Funct. Mater.,* 2010, **20**(24), 4250-4257.
33. R. Weissleder, *Nat. Biotechnol.,* 2001, **19**(4), 316-317.
34. L. Du, J. Li, C. Chen, Y. Liu, *Free Radic. Res.,* 2014, **48**(9), 1061-1069.
35. A. Teleki, M. C. Heine, F. Krumeich, M. K. Akhtar, S. E. Pratsinis, *Langmuir,* 2008, **24**(21), 12553-12558.
36. D. Villano, M. S. Fernandez-Pachon, M. L. Moya, A. M. Troncoso, M. C. Garcia-Parrilla, *Talanta,* 2007, **71**(1), 230-235.
37. G. Mitrikas, Y. Deligiannakis, C. C. Trapalis, N. Boukos, G. Kordas, *J. Sol-Gel Sci. Technol.,* 1998, **13**(1-3), 503-508.
38. M. Shanthil, R. Thomas, R. S. Swathi, K. George Thomas, *J. Phys. Chem. Lett.,* 2012, **3**(11), 1459-1464.
39. G. A. Sotiriou, F. Starsich, A. Dasargyri, M. C. Wurnig, F. Krumeich, A. Boss, J.-C. Leroux, S. E. Pratsinis, *Adv. Funct. Mater.,* 2014, **24**(19), 2818-2827.
40. U. Kreibig, L. Genzel, *Surf. Sci.,* 1985, **156**(JUN), 678-700.

41. A. M. Elliott, R. J. Stafford, J. Schwartz, J. Wang, A. M. Shetty, C. Bourgoyne, P. O'Neal, J. D. Hazle, *Med. Phys.,* 2007, **34**(7), 3102-3108.
42. C.-W. Yen, M. A. El-Sayed, *J. Phys. Chem. C,* 2009, **113**(45), 19585-19590.
43. M. C. Foti, C. Daquino, C. Geraci, *J. Org. Chem.,* 2004, **69**(7), 2309-2314.
44. S. Sanchez-Cortes, J. V. Garcia-Ramos, *J. Colloid Interface Sci.,* 2000, **231**(1), 98-106.
45. R. A. Alvarez-Puebla, *J. Phys. Chem. Lett.,* 2012, **3**(7), 857-866.
46. D. D. Evanoff, G. Chumanov, *ChemPhysChem,* 2005, **6**(7), 1221-1231.

Figure captions

Figure 1. High-resolution electron microscopy of as-prepared (a) and GA functionalized SiO_2-coated Ag nanoparticles (b). (c) X-ray diffraction patterns of the as-prepared (black line) and the functionalized (red line) SiO_2-coated Ag nanoparticles. The average crystal size as determined by Rietveld analysis and a representative schematic of the hybrid plasmonic nanoantioxidant is also shown.

Figure 2. (a) Optical absorption spectra of methanol suspensions containing as-prepared (black line) and GA functionalized (red line) SiO_2-coated Ag nanoparticles (particle concentration 0.1 mg/mL). The insets show photos of the suspensions respectively. (b) Bulk temperature of methanol suspensions containing 0.01 - 0.2 mg/mL of the functionalized SiO_2-coated Ag nanoparticles as a function of time for laser radiative flux (power per area) of 11.7 W/cm^2. The arrows signify the laser on/off time. The insets show the infrared camera images of each solution at t = 150 s.

Figure 3. (a) EPR spectra and (b) UV-vis spectra for GA functionalized SiO_2-coated Ag nanoparticles (red line) and time dependence of DPPH$^\bullet$ in the presence of GA-functionalized SiO_2-coated Ag nanoparticles for reaction time t = 0 - 60 min (dark purple to light purple) at room temperature. (c) The DPPH$^\bullet$ decay kinetics of the SiO_2-coated Ag nanoparticles functionalized with GA at room temperature (black line), during 785 nm laser pulses (10 s) (red line), and bulk heating at 35 (green line) and 40 ˚C (blue line). (d) The reaction kinetic rates for the DPPH$^\bullet$ decay as a function of the laser radiative flux (power per area). Error bars (n = 3) are smaller than symbols.

Figure 4. Raman spectra for GA, SiO_2-coated Ag nanoparticles and GA functionalized SiO_2 coated Ag nanoparticles recorded using a 785 nm laser excitation. The laser power that was employed for each spectrum is also shown.

Scheme 1. Reaction mechanism for the Proton Coupled Electron Transfer from the phenolic OH of grafted GA to a DPPH radical (a) without irradiation, (b) under 785 nm laser irradiation. In both cases the rate-limiting step is the formation of an activated transient state (TS) intermediate that involves association between DPPH$^\bullet$ and GA. The HAT process proceeds via this TS, and its kinetics is also affected by the

surrounding solvent molecules. In (b), upon near-IR 785 nm laser excitation, the plasmonic resonance of the Ag core produces strong vibrating local electric fields that lower the activation energy E_a by at least 2 kcal/mole.

Figures

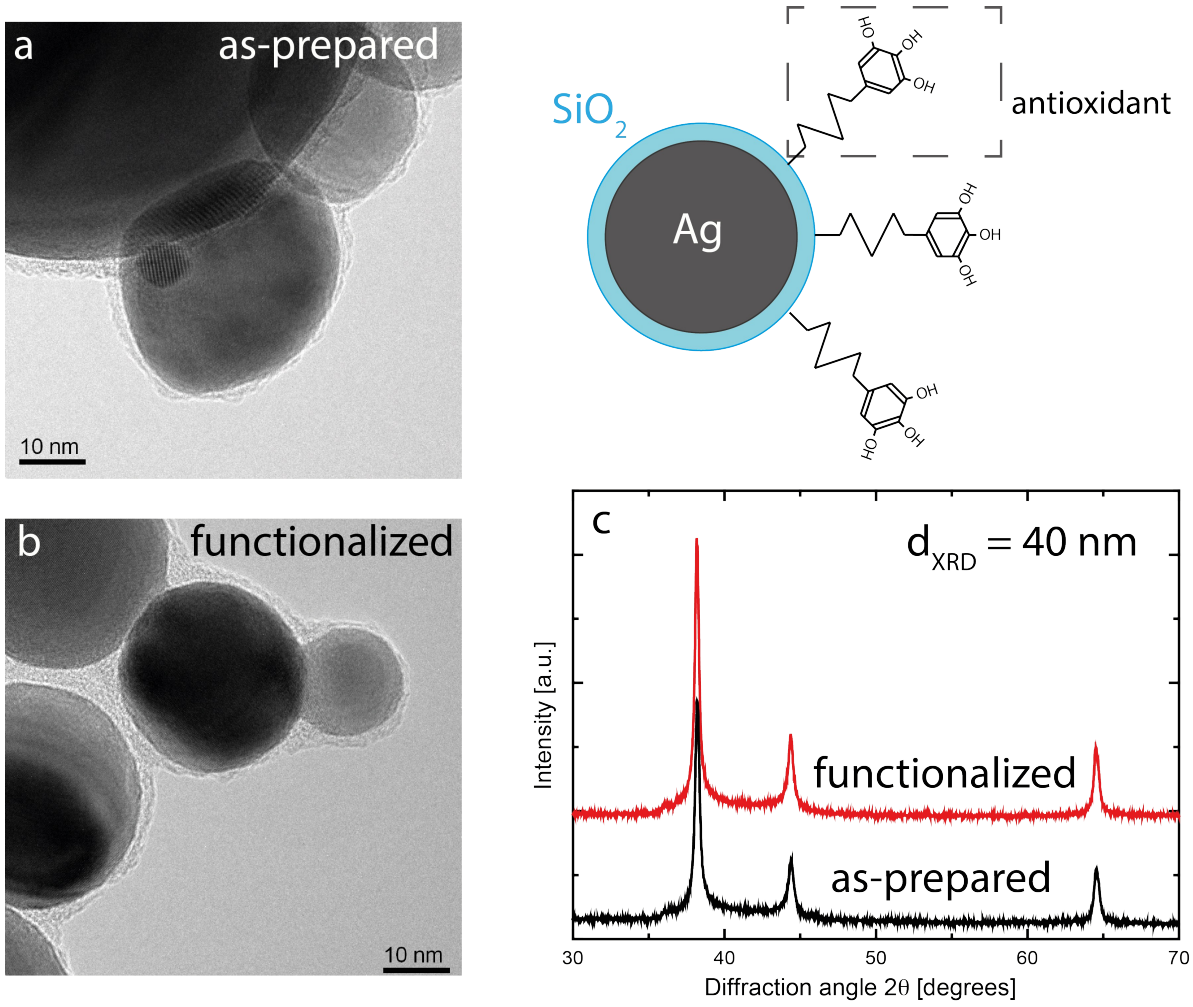

Figure 1

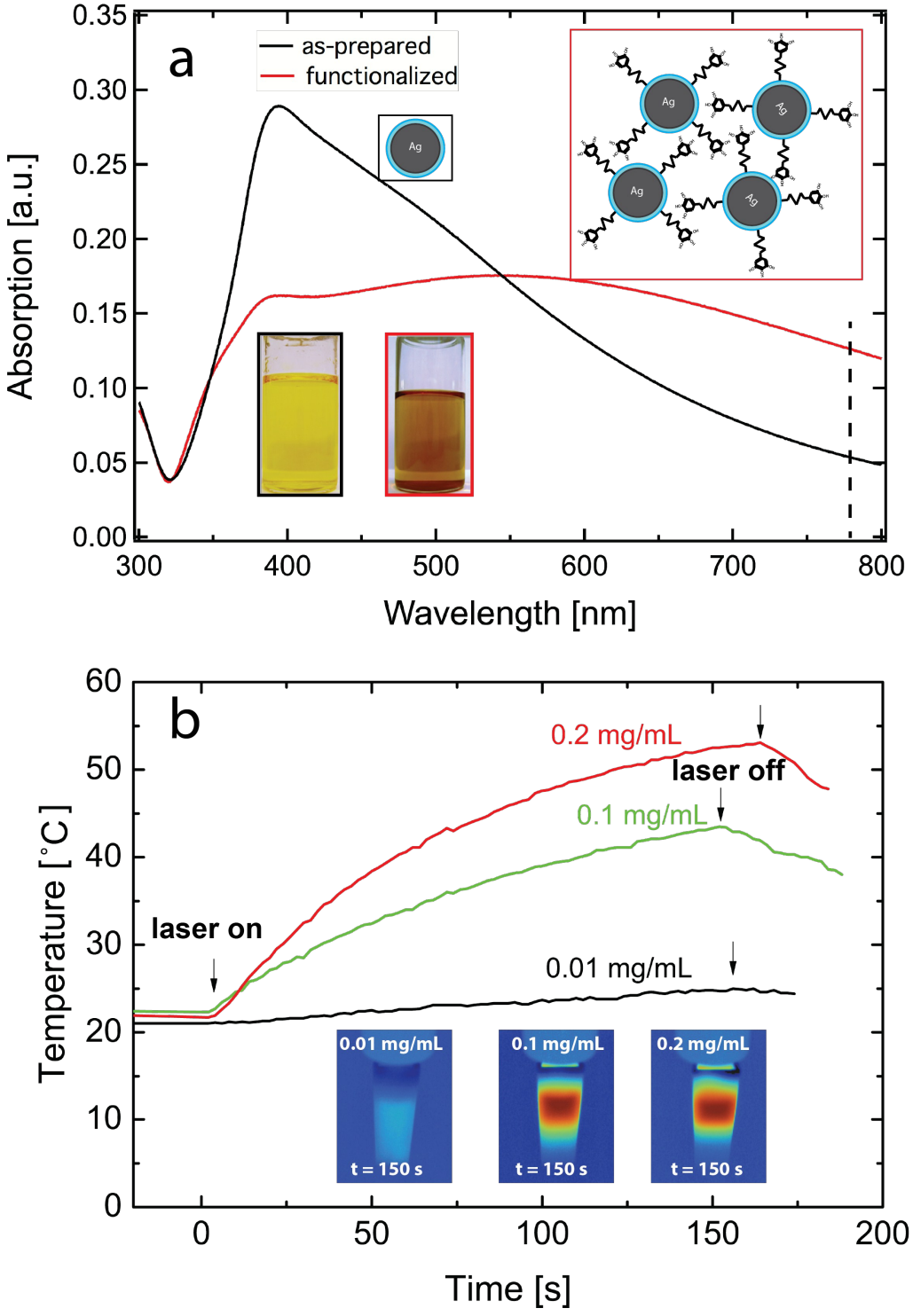

Figure 2

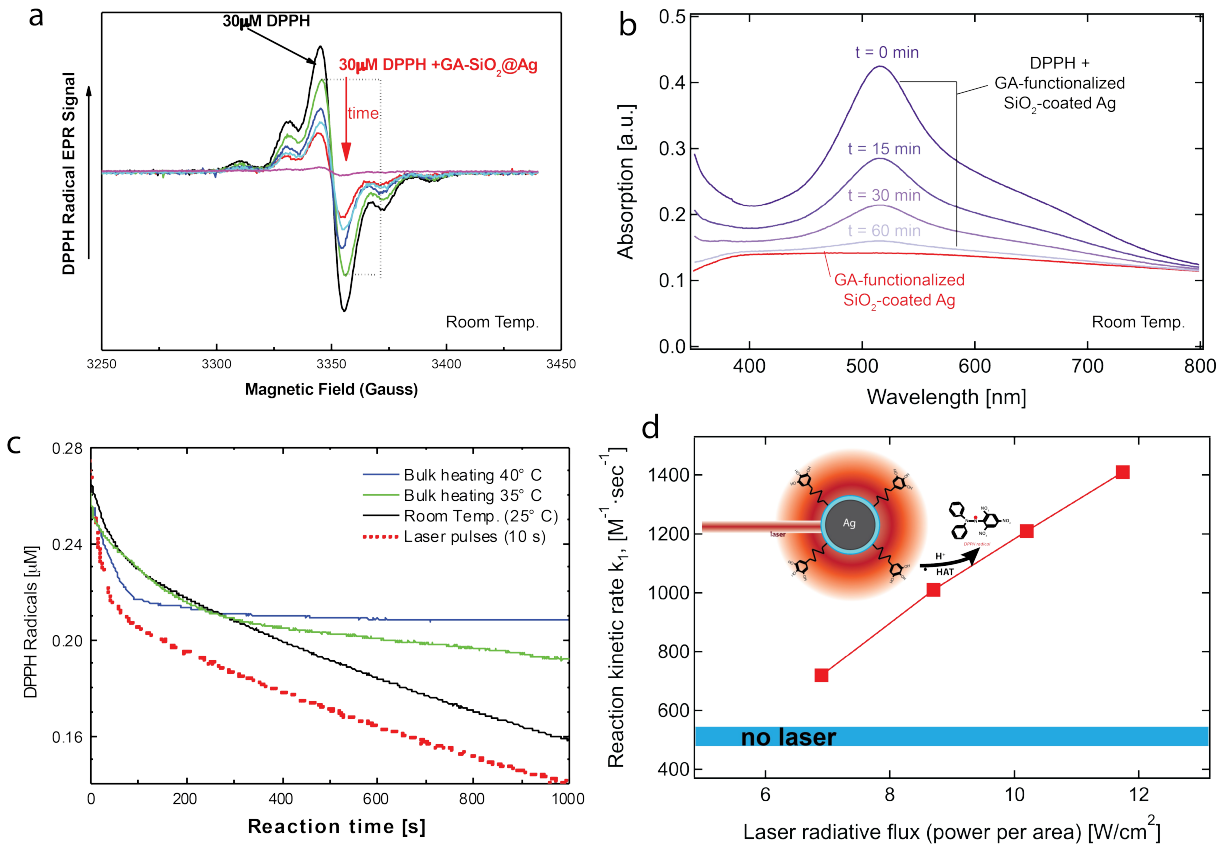

Figure 3

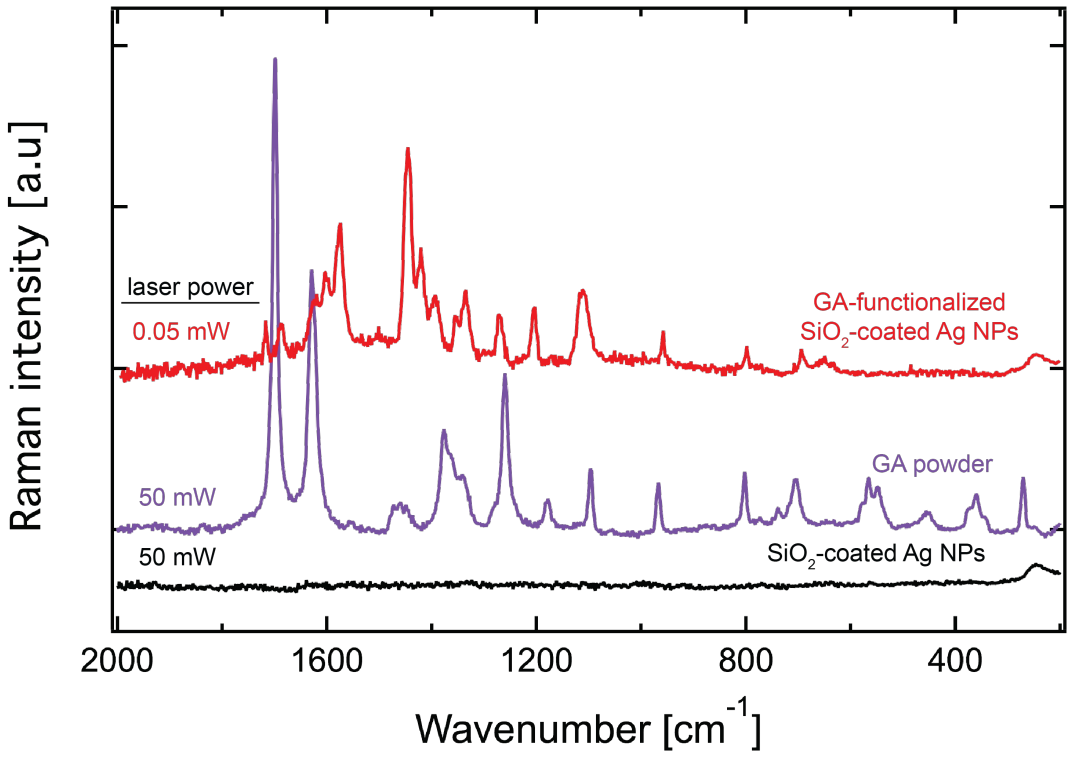

Figure 4

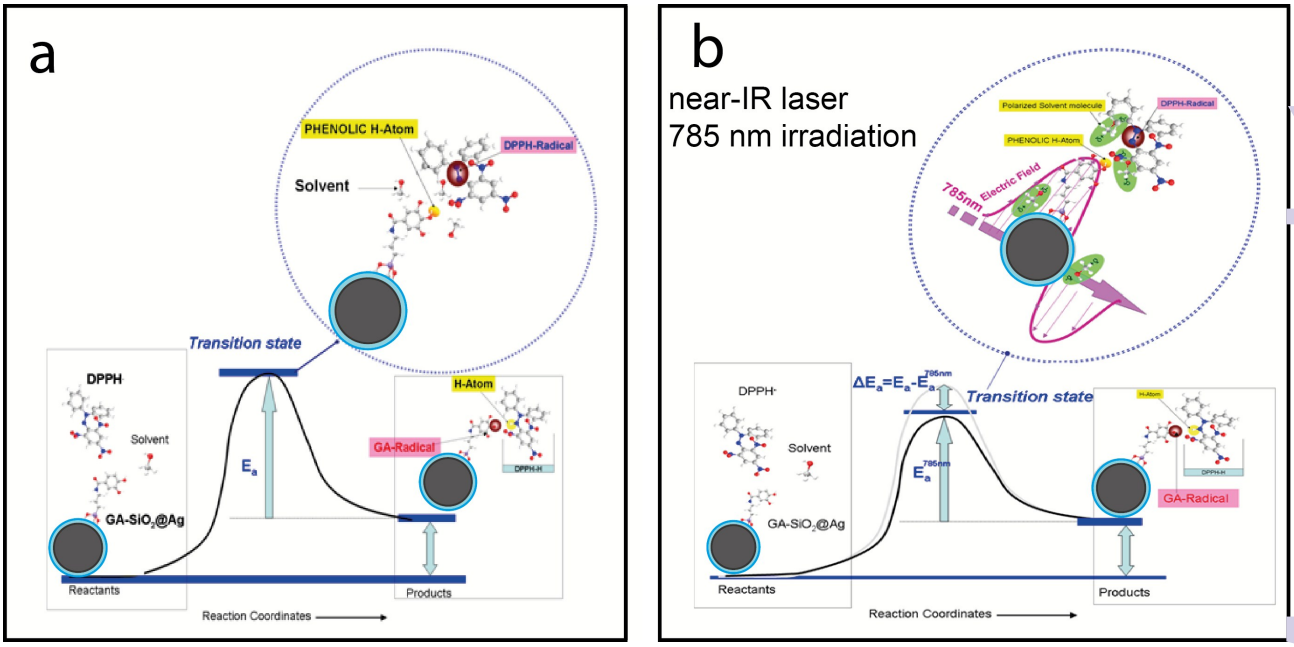

Scheme 1